

Time-Resolved Fluorescence (TRF) and Diffuse Reflectance Spectroscopy (DRS) for Margin Analysis in Breast Cancer

Nourhan Shalaby,^{1*} Alia Al-Ebraheem,¹ Du Le,¹ Sylvie Cornacchi,² Qiyin Fang,³ Thomas Farrell,⁴ Peter Lovrics,^{2,5} Gabriela Gohla,^{5,6} Susan Reid,⁴ Nicole Hodgson,⁴ and Michael Farquharson¹

¹School of Interdisciplinary Science, McMaster University, Ontario, Canada

²Faculty of Health Sciences, Department of Surgery, McMaster University, Hamilton, Ontario, Canada

³Faculty of Engineering, McMaster University, Hamilton, Ontario, Canada

⁴Juravinski Hospital and Cancer Centre, Hamilton, Ontario, Canada

⁵St. Joseph's Healthcare, Hamilton, Ontario, Canada

⁶Department of Pathology and Molecular Medicine, McMaster University, Hamilton, Ontario, Canada

Purpose: One of the major problems in breast cancer surgery is defining surgical margins and establishing complete tumor excision within a single surgical procedure. The goal of this work is to establish instrumentation that can differentiate between tumor and normal breast tissue with the potential to be implemented *in vivo* during a surgical procedure.

Methods: A time-resolved fluorescence and reflectance spectroscopy (tr-FRS) system is used to measure fluorescence intensity and lifetime as well as collect diffuse reflectance (DR) of breast tissue, which can subsequently be used to extract optical properties (absorption and reduced scatter coefficient) of the tissue. The tr-FRS data obtained from patients with Invasive Ductal Carcinoma (IDC) whom have undergone lumpectomy and mastectomy surgeries is presented. A preliminary study was conducted to determine the validity of using banked pre-frozen breast tissue samples to study the fluorescence response and optical properties. Once the validity was established, the tr-FRS system was used on a data-set of 40 pre-frozen matched pair cases to differentiate between tumor and normal breast tissue. All measurements have been conducted on excised normal and tumor breast samples post surgery.

Results: Our results showed the process of freezing and thawing did not cause any significant differences between fresh and pre-frozen normal or tumor breast tissue. The tr-FRS optical data obtained from 40 banked matched pairs showed significant differences between normal and tumor breast tissue.

Conclusion: The work detailed in the main study showed the tr-FRS system has the potential to differentiate malignant from normal breast tissue in women undergoing surgery for known invasive ductal carcinoma. With further work, this successful outcome may result in the development of an accurate intraoperative real-time margin assessment system. *Lasers Surg. Med.* 50:236–245, 2018. © 2018 Wiley Periodicals, Inc.

Key words: optical spectroscopy; margin assessment; fluorescence; diffuse reflectance; absorption coefficient; reduced scatter coefficient

INTRODUCTION

Breast cancer is accountable for 13% of female cancer deaths in Canada and remains the most frequently diagnosed cancer in women [1]. Early stage cancers are managed with breast conserving surgery where surgeons aim to remove the identified cancer along with a rim of normal tissue of 1–2 mm to confirm complete cancer removal. Margin detection between tumor and normal tissue has proven to be a problematic challenge for surgeons. Thus, surgical margin assessment is an area of great relevance and active research in breast cancer. The presence of a clear surgical margin is the most important indicator available to ensure completeness of surgical excision, while a positive surgical margin is a significant risk factor for predicting local recurrence. Furthermore, the presence of positive margins, which can be up to 30% [2], generally leads to further surgical resections with associated morbidity, resource utilization, anxiety, and delay. Optical biopsies have been recently used to potentially replace the current assessments where a pathologist examines the rim of normal tissue around the cancer to confirm it is clear of any cancer cells as the current pathological assessment remains time consuming and labor intensive and is not readily transferable to routine practice [3–11].

In this study a time-resolved fluorescence and reflectance spectroscopy (tr-FRS) system is utilized to study samples obtained from patients with breast Invasive

Conflict of Interest Disclosures: All authors have completed and submitted the ICMJE Form for Disclosure of Potential Conflicts of Interest and none were reported.

Contract grant sponsor: Juravinski Hospital and Cancer Centre Foundation Fall 2014 Research Grant.

*Correspondence to: Nourhan Shalaby, Department of Interdisciplinary Science, McMaster University, 1280 Main Street West, Hamilton, Ontario, L8S 4L8 Canada.

E-mail: shalabyn@mcmaster.ca

Accepted 31 December 2017

Published online 22 January 2018 in Wiley Online Library

(wileyonlinelibrary.com).

DOI 10.1002/lsm.22795

Ductal Carcinoma (IDC) whom have undergone lumpectomy or mastectomy. By measuring fluorescence intensity and lifetime as well as collecting diffuse reflectance (DR) of the tissue, the data can subsequently be used to extract optical properties (absorption and reduced scatter coefficient) of the tissue.

Time-resolved fluorescence (TRF) measures the fluorescence lifetime and fluorescence intensity response in endogenous fluorophores present within the tissue. Endogenous fluorophores of particular interest in breast tissue include collagen, reduced nicotinamide adenine dinucleotide (NADH), and flavin adenine dinucleotide (FAD). The NADH/FAD red-ox state of the tissue has also been examined in previous work [12] and has been shown to be significantly higher in tumor versus normal breast tissue. The TRF technique has been performed to distinguish between glioma specimens from normal tissue [13–15]. Fluorescence lifetime is an intrinsic feature of fluorophores. Fluorescence lifetime is the time required by a population of excited fluorophores to decrease exponentially to N/e or 36.8% of initial population (N) via the energy loss through fluorescence and other non-radiative processes. Endogenous fluorophores have lifetimes that can vary from picoseconds to nanoseconds [16]. Fluorescence lifetime is independent of biological relevant fluorophore concentration, absorption by the sample, fluorescence intensity, photo-bleaching, and/or excitation intensity.

Diffuse reflectance (DR) uses a broadband light source in the UV-VIS region providing illumination and the diffuse reflectance spectra is collected by detection fibers positioned at various distances from the source fiber. The diffuse reflectance can interpret how light is either back scattered or absorbed from tissue. The diffuse reflectance can display absorption and scattering properties of the tissue, revealing physiological and morphological changes, respectively. The absorption coefficient can reveal information on major absorbers in the tissue, such as oxygenated and deoxygenated hemoglobin and beta-carotene, while the reduced scatter coefficient can relay information on the size and density of scattering centers,

such as nuclei and cells, in the tissue. The optical properties at 545 and 575 nm will be investigated in this work as they correspond to the absorption peaks of oxygenated hemoglobin which has been shown to be altered in tumor lesion [17].

The preliminary aim of this work is to compare between fresh and pre-frozen breast tissue to assess the effects of the freezing and thawing process on the tr-FRS parameters to validate the use of pre-frozen tissue in further work. The primary aim is to evaluate whether the tr-FRS system is capable of differentiating between tumor and normal breast tissue. These aims serve towards the ultimate goal of establishing credible technology that can be used in a device with the potential of providing substantially higher confidence of accurate and complete tumor removal within a single surgical procedure *in vivo* in real time.

METHODS

Samples

Matched pair breast samples were collected from St. Joseph's Healthcare and the Juravinski Hospital and Cancer Centre directly after surgery and subsequently measured using the tr-FRS system. A small piece of excised tumor tissue was provided from surgery, with a minimum size requirement of $4 \times 3 \times 2$ mm. A further small piece of normal tissue, from the same patient, with equivalent size was excised at a distance from the tumor area to avoid any boundary effects. Furthermore, histological analysis was performed to confirm normal specimens were free of any tumor content. Measurements were made on post-surgical excised samples at three different locations as illustrated in Figure 1 and each measurement was repeated three times. The data presented in this work represents the average of all measurements made on each sample. The protocol and study processes were approved and performed in accordance with the recommendations and regulations of "Hamilton Integrated Research Ethics Board."

Preliminary study-sample set. Ten matched pair IDC specimens were collected and directly measured with the tr-FRS system within 30 minutes after surgery to extract

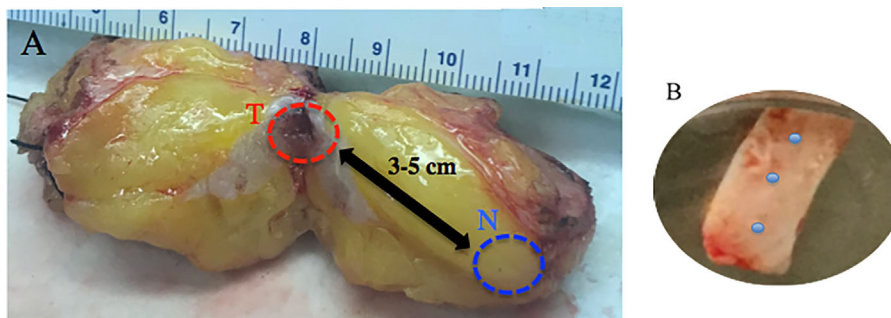


Fig. 1. (A) A breast specimen that has undergone lumpectomy showing the locations of excision with a distance of 3–5 cm between tumor and normal. (B) An image of an excised tumor breast specimen. Blue dots represent the approximate measurement locations, where each location was measured three times.

the optical parameters. After data collection, the fresh tissues were frozen from room temperature to a freezer with subzero temperature of -80°C for a period of time between 4 and 6 weeks. After this time, data collection was repeated subsequent to complete thawing of the tissue samples. This temperature was chosen to avoid mechanical changes proven to cause Collagen damage with use of snap freezing using liquid nitrogen (-196°C) [18]. Exposing tissue to room temperature for a few minutes allowed the thawing process to be completed without any external interference or further processing. Comparison was carried out to investigate if there were differences in the data from samples when collected from the fresh tissues and after the same tissue had been frozen.

Main study-sample set. Forty matched pair IDC pre-frozen banked specimens were stored in a freezer with subzero temperature of -80°C until time of measurement.

Methodology

An integrated, dual-modality tr-FRS instrument was used to collect intrinsic fluorescence and reflectance data from the specimens. The TRF spectroscopy measures fluorescence intensity and lifetime of fluorophores, providing information on biological composition of tissue [16,19,20]. DRS reveal optical properties that relay information on absorber concentration as well as scattering size, structure, and density of cells [17,21,22]. Although both techniques have been used separately to classify tissue types, the integration of both modalities allows the yield of higher sensitivity and specificity than each modality alone. Figure 2 shows the integration of the two subsystems. The TRF module uses a UV pulsed laser source at 355 nm and pulse width of 0.3 ns (PNV-001525-140, Teem Photonics, Meylan, France) to excite endogenous tissue fluorophores and collect the spectral

fluorescence intensity and lifetime response of breast tissue with a range 350–550 nm. An acousto-optic tunable filter (AOTF, TEAF5-0.36–0.52-S, Brimrose, MD) is used to apply rapid wavelength switch while a photomultiplier tube and a high-speed digitizer are used to retrieve decay at each wavelength in real time [19,23]. In the DRS subsystem, a broadband light source (Dolan-Jenner MI-150, Edmund Optics, NJ) is used to illuminate the sample and diffuse reflectance from 300 to 800 nm at various source-detector distances (0.23, 0.59, and 1.67 mm) are collected. A fiber optic probe of 2 mm diameter (illustrated in Fig. 3) is used to integrate both excitation sources and collect the output signal from the TRF and DRS in a hand-held device. For more information on the system, please refer to the methods section described by Nie et al. [15].

All statistical analysis was performed using IBM SPSS Statistics Version 22. The P -value has been reported as significant for each variable as $P < 0.05$. The Shapiro-test was used for each category to test if the data set was consistent with a Gaussian distribution function. Wilcoxon Signed Ranks Test was used for comparing the difference of the parameters for non-normally distributed data while Paired-Sample T Test was used for normally distributed data.

RESULTS

Preliminary Study-Results

TRF results.

Fluorophore lifetime. Table 1 compares fresh with pre-frozen in both normal and tumor breast tissue at 400, 460, and 515 nm, corresponding to the emission wavelength of the endogenous fluorophores Collagen, NADH, and FAD respectively. No significant difference was observed between the fresh and pre-frozen samples in normal and tumor samples. This suggests that the freezing and

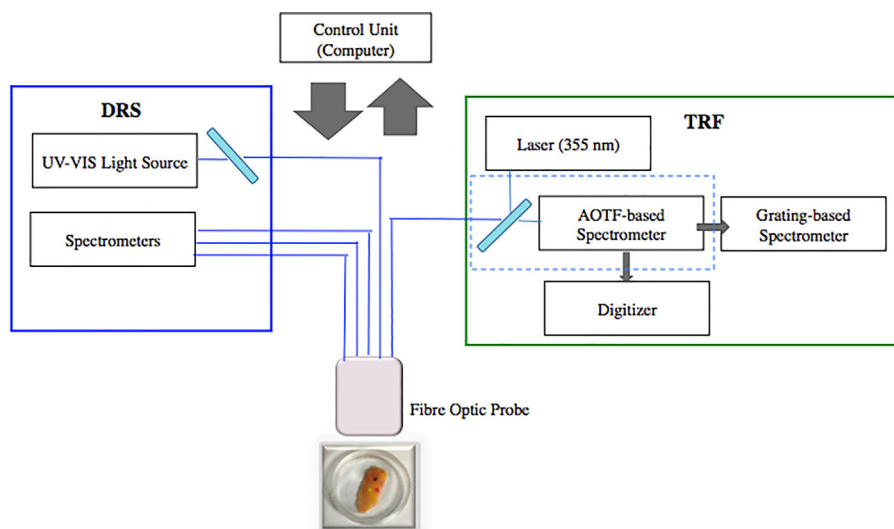


Fig. 2. An illustration of the integration of the DRS subsystem (left) and the TRF subsystem (right) with data collection occurring through a probe and a central control unit (computer).

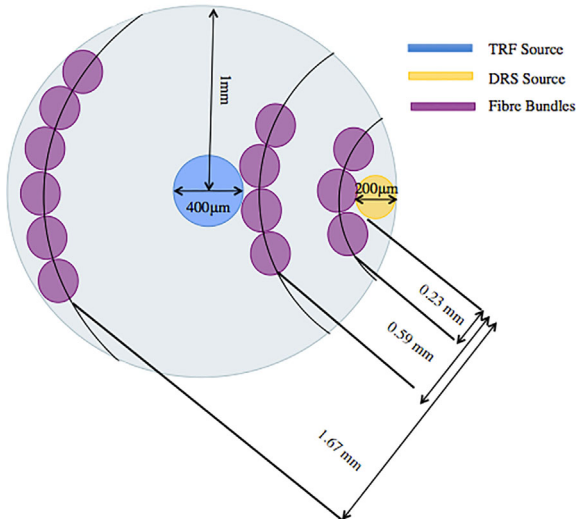


Fig. 3. Transverse view of fiber optic probe. All fibers are 0.23 mm, unless indicated otherwise.

thawing process did not yield significant changes on the fluorescence lifetime.

Fluorophore intensity. Figure 4 compares fluorescence intensity spectra for (A) fresh to pre-frozen normal samples and (B) fresh to pre-frozen tumor samples. All spectra are normalized to the applied voltage and are represented as arbitrary units with the maximum value as the NADH peak value at 460 nm. The spectra were analyzed using Peak Fit software (PeakFit TM v.4.12, Seasolve Software Inc.) where the emission peaks of fluorophores (collagen at 400 nm, NADH at 460 nm, and FAD at 515 nm) were smoothed and treated as Gaussian distributions to determine the amplitude, FWHM and integral area of each fluorophore. For each peak, the integral area was determined by PeakFit using the following FWHM and amplitude equation:

$$y = a \exp\left(-\ln(2) \left(\frac{x - x_0}{dx}\right)^2\right)$$

where a is the amplitude represented in arbitrary units, dx is the half width at half maximum (HWHM) and x_0 is the maximum position.

Collagen. Table 2 shows collagen integral area in freshly excised and pre-frozen between normal and tumor breast tissue ($n = 10$).

FAD. Table 3 shows FAD integral area in freshly excised and pre-frozen between normal and tumor breast tissue ($n = 10$).

NADH / FAD. Table 4 shows NADH/FAD integral area in freshly excised and pre-frozen between normal and tumor breast tissue ($n = 10$).

Tables 2–4 show no significant difference between fresh and pre-frozen collagen, FAD and NADH/FAD integral area in both normal and tumor breast tissue.

DR results.

Optical properties. Table 5 compares the absorption coefficient between fresh and pre-frozen normal and tumor breast tissue at 545 and 575 nm. No significant difference was observed for both the normal and tumor subset.

Reduced scatter coefficient. Table 6 compares the reduced scatter coefficient between fresh and pre-frozen in both normal and tumor breast tissue at 545 and 575 nm.

No significant differences in absorption coefficient and reduced scatter coefficient were observed for both the normal and tumor subset in Tables 5 and 6. This implies that the freezing and thawing process did not contribute to significant differences in optical properties. In both Tables 5 and 6 power analysis has been performed to determine the strength of the sample size on the significance level and yielded in low power which can be contributed to the small sample size used in this sub-study.

Main Study-Results

TRF results.

Fluorophore lifetime. Table 7 shows the lifetime values at 400, 460, and 515 nm, the wavelength corresponding to collagen, NADH and FAD emissions, respectively.

Fluorophore intensity. Normalization and fitting of the fluorescence intensity was performed as mentioned above. Figure 5 compares the fluorescence intensity of 40 matched pair cases of normal and tumor breast samples.

TABLE 1. Lifetime at 400, 460, 515 nm in Freshly Excised and Pre-Frozen Normal and Tumor Breast Samples ($n = 10$)

	Normal			Tumor		
	Mean (ns)	Standard error	P -value	Mean (ns)	Standard error	P -value
Fresh lifetime 400 nm	3.126	0.194	$P = 0.303^a$	4.381	0.179	$P = 0.055^a$
Pre-frozen lifetime 400 nm	3.391	0.247		4.921	0.228	
Fresh lifetime 460 nm	6.605	0.266	$P = 0.664^a$	5.334	0.341	$P = 0.878^b$
Pre-frozen lifetime 460 nm	6.711	0.311		5.495	0.323	
Fresh lifetime 515 nm	8.255	0.451	$P = 0.249^a$	5.818	0.508	$P = 0.721^b$
Pre-frozen lifetime 515 nm	7.830	0.491		5.841	0.510	

^aPaired-Samples t -test.

^bWilcoxon Signed Ranks test. Significance tested at $P < 0.05$.

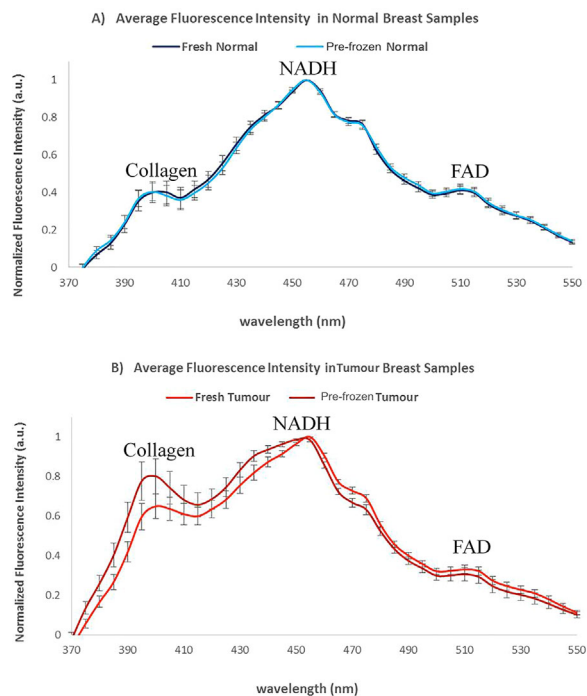


Fig. 4. A direct comparison between freshly excised and pre-frozen normal breast tissue is demonstrated in Figure 4A followed by freshly excised and pre-frozen tumor breast tissue in Figure 4B. Errors are SE of the mean.

Collagen. Table 8 shows the collagen integral area between normal and tumor breast samples.

DR Results. Figure 6 displays the average diffuse reflectance spectra from fiber 1 between normal and tumor breast samples from the 420 to 670 nm range.

In Table 9 below, the average diffuse reflectance from fiber 1 at 545 and 575 nm, the wavelengths corresponding to the absorption of hemoglobin, is shown.

Optical properties.

Absorption coefficient. Figure 7 below displays the average absorption coefficient from 480 to 620 nm between normal and tumor breast samples.

TABLE 2. Collagen Integral Area in Freshly Excised and Pre-Frozen Normal and Tumor Breast Tissue ($n = 10$)

	Mean	Std. error	P -value
Fresh normal collagen area	10.227	1.807	$P = 0.988^a$
Pre-frozen normal collagen area	10.199	1.702	
Fresh tumor collagen area	20.035	2.862	$P = 0.280^b$
Pre-frozen tumor collagen area	23.528	3.038	

^aPaired-Samples t -test.

^bSignificance tested at $P < 0.05$.

TABLE 3. FAD Integral Area in Freshly Excised and Pre-Frozen Normal and Tumor Breast Tissue ($n = 10$)

	Mean	Std. error	P -value
Fresh normal FAD area	16.777	0.882	$P = 0.463^a$
Pre-frozen normal FAD area	17.655	1.379	
Fresh tumor FAD area	15.208	1.356	$P = 0.386^b$
Pre-frozen tumor FAD area	13.671	1.829	

^aPaired-Samples t -test.

^bWilcoxon Signed Ranks test.

Significance tested at $P < 0.05$.

Table 10 represents the average absorption coefficient in normal and tumor breast samples at 545 and 575 nm.

Reduced scatter coefficient. Figure 8 displays the average reduced scatter coefficient from 480 to 620 nm between normal and tumor breast samples.

Table 11 presents the reduced scatter coefficient in normal and tumor breast samples at 545 and 575 nm.

DISCUSSION

Preliminary Study

Several groups have used steady-state fluorescence and diffused reflectance to investigate the cryogenic effects on soft tissue. In one study it was reported that there was no significant deviation in *ex vivo* fluorescence intensity upon freezing and thawing of rodent cheek pouch tissue but rather a significant change in the diffuse reflectance measurements can be observed [24]. The study attributed this to changes in hemoglobin and oxygen content in the pre-frozen samples. Other work [25] compared optical properties between intact soft tissue and defrosted tissue paste of calf aorta, rat jejunum, and rabbit sciatic nerve and found no significant differences between the optical properties. An earlier study investigated the effects of freezing and thawing on the optical properties of human aorta and reported a significant decrease in absorption coefficient over the 300–800 nm range and reduced scatter coefficient in a smaller range from 300 to 335 nm [26].

TABLE 4. NADH/FAD Integral Area in Freshly Excised and Pre-Frozen Normal and Tumor Breast Tissue ($n = 10$)

	Mean	Std. error	P -value
Fresh normal NADH to FADH area	3.483	0.187	$P = 0.878^a$
Pre-frozen normal NADH to FADH area	3.432	0.372	
Fresh tumor NADH to FADH area	3.906	0.401	$P = 0.213^a$
Pre-frozen tumor NADH to FADH area	4.687	0.497	

^aPaired-Samples t -test.

Significance tested at $P < 0.05$.

TABLE 5. Absorption Coefficient at 545 and 575 nm for Fresh and Pre-Frozen Normal and Tumor Breast Tissue ($n = 10$)

	Normal				Tumor			
	Mean (cm^{-1})	Standard error	<i>P</i> -value	Power analysis	Mean (cm^{-1})	Standard error	<i>P</i> -value	Power analysis
Fresh absorption coefficient 545 nm	5.735	1.281	$P = 0.434^a$	0.078	5.208	0.624	$P = 0.128^a$	0.216
Pre-frozen absorption coefficient 545 nm	6.598	1.188			7.141	1.528		
Fresh absorption coefficient 575 nm	6.033	1.389	$P = 0.591^a$	0.065	5.229	0.623	$P = 0.139^b$	0.252
Pre-frozen absorption coefficient 575 nm	6.702	1.265			7.507	1.651		

^aPaired-Samples *t*-test.^bWilcoxon Signed Ranks test.

Our results have indicated that the process of freezing and thawing did not cause any significant differences between fresh and pre-frozen breast tissue in both normal and tumor breast tissue for fluorescence lifetime at 400, 460, and 515 nm as well as collagen peak area, FAD peak area, NADH/FAD peak area, absorption coefficient at 545 and 575 nm as well as the reduced scatter coefficient at 545 and 575 nm. This justifies the suitability of using banked frozen tissue bank specimens in our work. The fact that our study used different tissue types and followed a different method of sample preparation involving no grinding or physical changes to the tissue, would explain the discrepancies between other studies and does not allow for direct comparison as no significant differences in absorption were observed in our study.

Main Study

Fluorophore lifetime. There has been a range of values for collagen fluorescence and lifetime in the

literature [27,28]. However, the complexity of collagen fluorescence makes it harder to differentiate between collagen types I, II, and III in the 390–410 nm emission range. Although classification of different collagen types is difficult, most studies have reported higher collagen fibrils and thus longer collagen lifetimes in diseased states in comparison to healthy states, verifying our results of significantly higher tumor lifetime (4.3 ns) compared to normal collagen at (3.5 ns) at the wavelength of 400 nm corresponding to collagen emission, as shown in Table 7.

NADH has a mean fluorescence lifetime ranging from 0.2 to 0.4 ns in its free state. However, when NADH is protein bound, it will exhibit longer lifetimes typically in the ~2.5–3.4 ns range. As per Table 7, our measured response at 460 nm, attributed mainly to NADH, was 6.3 and 5.1 ns for normal and tumor breast tissue respectively, higher than the reported protein bound NADH lifetime. A study by Skala et al. reported significantly decreased ($P < 0.05$) protein-bound NADH in tumor tissue compared

TABLE 6. Reduced Scatter Coefficient at 545 nm and 575 nm for Fresh and Pre-Frozen Normal and Tumor Breast Tissue ($n = 10$)

	Normal				Tumor			
	Mean (cm^{-1})	Standard error	<i>P</i> -value	Power analysis	Mean (cm^{-1})	Standard error	<i>P</i> -value	Power analysis
Fresh reduced scatter coefficient 545 nm	15.814	1.745	$P = 0.210^a$	0.118	17.310	1.415	$P = 0.05^b$	0.583
Pre-frozen reduced scatter coefficient 545 nm	17.756	1.869			21.952	1.607		
Fresh reduced scatter coefficient 575 nm	15.180	1.675	$P = 0.210^a$	0.119	16.616	1.358	$P = 0.05^b$	0.584
Pre-frozen reduced scatter coefficient 575 nm	17.044	1.794			21.072	1.542		

^aPaired-Samples *t*-test.^bWilcoxon Signed Ranks test.
Significance tested at $P < 0.05$.

TABLE 7. Lifetime at 400, 460, 515 nm in Pre-Frozen Normal and Tumor Breast Samples ($n = 40$)

	Mean (ns)	Std. error	P -value
Normal lifetime 400 nm	3.567	0.138	$P < 0.01^{*,b}$
Tumor lifetime 400 nm	4.318	0.205	
Normal lifetime 460 nm	6.342	0.172	$P < 0.01^{*,a}$
Tumor lifetime 460 nm	5.141	0.097	
Normal lifetime 515 nm	7.411	0.238	$P < 0.01^{*,a}$
Tumor lifetime 515 nm	5.261	0.138	

^aPaired-Samples t -test.

^bWilcoxon Signed Ranks test.

*Statistically significant at $P < 0.05$.

to normal tissue and attributed this change to a shift in metabolic conditions from oxidative phosphorylation to glycolysis in tumor prognosis [29].

Table 7 shows lower FAD lifetime in tumor of 5.2 ns compared to the normal 7.1 ns breast samples, which falls within the range of published data as free state FAD has been reported to have a decay time of 5 ns, with a faster lifetime of about 1 ns in the bound form [30]. Any changes in the NADH/FAD and their relative amounts of free and protein-bound states depend on the glycolysis and oxidative phosphorylation ratio. Since tumor progression results in a shift from oxidative phosphorylation to glycolysis, comparing short and long lifetime fluorescence decays of NADH and FAD can be used to discriminate between different metabolic conditions.

Fluorescence intensity. The increase of collagen deposition in malignant breast tissue has been observed in many previous studies [6,27,31–34]. Many have confirmed that increased density in breast correlates to higher incidences of breast cancers. This increase in breast

density can be attributed to increased fibril collagen deposition. All previous literature matches our results of significantly increased collagen content (integral area of 15.778 a.u.) at 400 nm in tumor compared to the normal (integral area of 9.746 a.u.) breast samples as per Figure 5 and Table 8.

Another major fluorescence component displaying significant differences between tumor and normal breast tissue at 460 nm is the emission of NADH. Like collagen, NADH is also found to be significantly higher in tumor compared to the normal breast samples [4,8,12,29,30]. NADH is one of the main coenzymes responsible for metabolic activities and the relative concentration of this coenzyme changes as the shift from oxidative phosphorylation to aerobic glycolysis is observed in the progression from normal to malignant state.

The third constituent of the emission spectra peaking at 510 nm in Figure 5 is attributed to FAD. Like NADH, FAD is another coenzyme responsible for cellular metabolism. The high-energy demands in breast cancer results in major metabolic reprogramming in the tumor state, affecting levels of FAD present within the cell. In normal conditions, NADH, acting as an electron donor, reduces FAD to FADH₂. After a series of intermediate reactions, FADH₂ is oxidized to FAD. However, in tumor development, the low oxygen concentrations prevent the conversion of FADH₂ to FAD, thereby resulting in lower levels of FAD in tumor breast compared to normal breast samples [35]. This explains the lower FAD content (integral area of 9.935 a.u.) observed in the tumor breast tissue samples compared to the normal FAD content (integral area of 13.659 a.u.) reported in our study (Table 8).

Although NADH and FAD values provide information on the metabolic state of the tissue, the ratio of NADH to FAD is a more accurate measurement as it provides a control for cell density and accounts for metabolic variation between a healthy and diseased cellular status. This red-ox ratio is important to monitor, as it is sensitive to cellular metabolic changes and oxygen depletion occurring during the progression of healthy to malignant state. As observed in this study, the increased NADH and decreased FAD levels observed in tumor tissue results in significantly increased NADH/FAD (integral area of 6.854 a.u.) red-ox levels compared to the normal NADH/FAD content (integral area of 4.88 a.u.) as shown in Table 8.

Diffuse reflectance. Numerous studies have used diffuse reflectance as an individual modality to discriminate between diseased and healthy tissue [7,24,36–38] and observed higher diffuse reflectance in tumor compared to normal breast tissue. This was consistent with our findings as shown in Table 9 and Figure 6 where higher DR was noted for tumor samples (0.409 a.u at 545 nm and 0.395 a.u. at 575 nm) when compared to normal breast samples (0.312 a.u at 545 nm and 0.306 a.u. at 575 nm).

Absorption coefficient. Although no significant differences were observed between the average

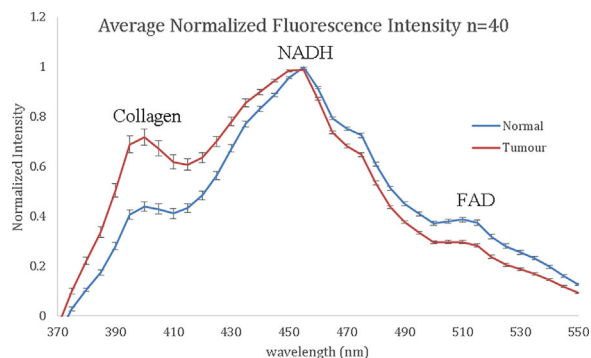
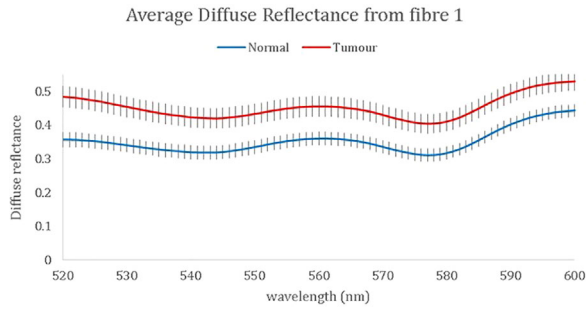
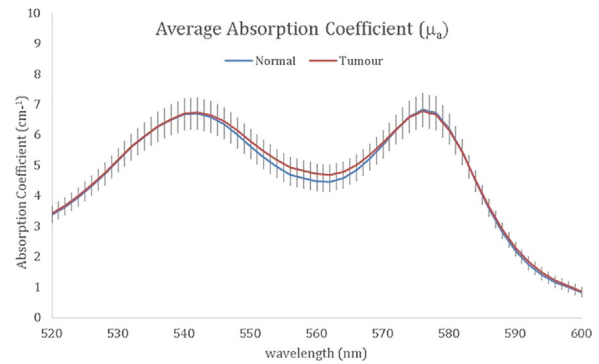


Fig. 5. Average fluorescence intensity in normal tumor breast samples ($n = 40$). Collagen produces an emission spectrum peaking at 390–400 nm, whereas reduced nicotinamide adenine dinucleotide (NADH), and flavin adenine dinucleotide (FAD) emit at 460 and 510 nm, respectively, when induced with a UV laser source of 355 nm. Emission peaks of collagen, NADH and FAD were taken at 400, 460, and at 510 nm, respectively. Errors are SE of the mean.

TABLE 8. Collagen, NADH, FAD, and NADH/FAD Integral Area in Normal and Tumor Breast Tissue Taken at 400 nm ($n = 40$)

	Mean (a.u.)	Std. error	P -value
Normal collagen area	9.746	0.661	$P < 0.01^{*,b}$
Tumor collagen area	15.778	0.899	
Normal NADH area	60.720	0.718	$P = 0.03^{*,a}$
Tumor NADH area	62.517	0.849	
Normal FAD area	13.659	0.609	$P < 0.01^{*,a}$
Tumor FAD area	9.935	0.429	
Normal NADH to FAD area	4.88	0.276	$P < 0.01^{*,b}$
Tumor NADH to FAD area	6.854	0.362	

^aPaired-Samples t -test.^bWilcoxon Signed Ranks test.*Statistically significant at $P < 0.05$.Fig. 6. Diffuse reflectance (DR) spectra of tumor and normal breast tissue from fiber 1 ($n = 40$). Tumor samples showing significantly higher DR than normal samples. Errors are SE of the mean.Fig. 7. The average absorption coefficient in normal and tumor breast samples ($n = 40$). Errors are SE of the mean.

absorption coefficient in tumor and normal samples in our study as shown in section 5.2.4.1 (Fig. 7 and Table 10), other studies found significantly higher absorption in normal compared to tumor tissue, especially at 545 and 575 nm, wavelengths corresponding to

oxygenated hemoglobin, the main absorber present in breast tissue. Zhu et al. [6] attributed the decrease in hemoglobin saturation in malignant breast tissue to the limited oxygen supply in the rapidly proliferating tumor cells. Zhu also noted significantly higher hemoglobin

TABLE 9. Diffuse Reflectance in Normal and Tumor Breast Samples at 545 and 575 nm ($n = 40$)

	Mean (a.u.)	Std. error	P -value
Normal diffuse reflectance 545 nm	0.312	0.018	$P < 0.01^{*,b}$
Tumor diffuse reflectance 545 nm	0.409	0.024	
Normal diffuse reflectance 575 nm	0.306	0.018	$P < 0.01^{*,a}$
Tumor diffuse reflectance 575 nm	0.395	0.023	

^aPaired-Samples t -test.^bWilcoxon Signed Ranks test.*Statistically significant at $P < 0.05$.**TABLE 10. Average Absorption Coefficient at 545 and 575 nm of Normal and Tumor Breast Tissue ($n = 40$)**

	Mean (cm^{-1})	Std. error	P -value
Normal absorption coefficient 545 nm	6.282	0.500	$P = 0.78^a$
Tumor absorption coefficient 545 nm	6.431	0.436	
Normal absorption coefficient 575 nm	6.484	0.531	$P = 0.81^b$
Tumor absorption coefficient 575 nm	6.654	0.472	

^aPaired-Samples t -test.^bWilcoxon Signed Ranks test.*Statistically significant at $P < 0.05$.

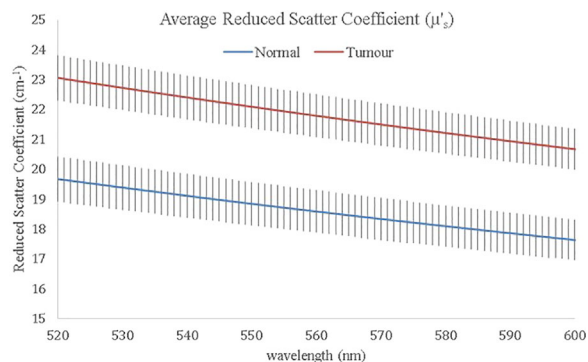


Fig. 8. The average reduced scatter coefficient in tumor and normal breast samples ($n = 40$). Errors are SE of the mean.

saturation in normal and benign tissue compared to malignant tumor.

Reduced scattering coefficient. The reduced scattering coefficient provides information on the scattering centers present in the biological tissue, such as the nuclei. Since increases in cellular proliferation and cell density is a hallmark of tumor progression, an increase in the reduced scattering coefficient is anticipated in tumor tissue. The reduced scattering coefficient was also shown to increase as a result of increased nuclear size, DNA content and hyperchromasia [39]. Significantly higher reduced scattering coefficient was observed in tumor (22.162 cm^{-1} at 545 nm and 21.273 cm^{-1} at 575 nm) compared to the normal breast tissue (18.571 cm^{-1} at 545 nm and 17.826 cm^{-1} at 575 nm) as per Table 11 and Figure 8, which was consistent with findings from previous studies [3,22,40,41]. Zhu et al. [6] noted that the reduced scatter coefficient was inversely correlated to the amount of adipose tissue present as well as the patient body mass index (BMI). The observed increase in the reduced scatter coefficient observed in this study could be linked to increased fibro-connective and glandular tissue content and thus cancer development.

TABLE 11. Average Reduced Scatter Coefficient at 545 and 575 nm of Normal and Tumor Breast Tissue ($n = 40$)

	Mean (cm^{-1})	Std. error	P-value
Normal reduced scatter coefficient 545 nm	18.571	0.790	$P < 0.01^{*,a}$
Tumor reduced scatter coefficient 545 nm	22.162	0.721	
Normal reduced scatter coefficient 575 nm	17.826	0.789	$P < 0.01^{*,a}$
Tumor reduced scatter coefficient 575 nm	21.273	0.692	

^aPaired-Samples t -test.

*Statistically significant at $P < 0.05$.

CONCLUSION

The preliminary study indicates the validity of using banked pre-frozen tissue to study the optical parameters required in distinguishing between normal and tumor breast samples. The time-resolved fluorescence and diffuse reflectance spectroscopy system was also used to discriminate between normal and tumor breast samples in 40 matches pair cases. The fluorescence intensity was used to provide information on the endogenous fluorophores collagen, NADH and FAD. The diffuse reflectance was used to reveal tissue optical properties; the absorption and reduced scatter coefficient. Statistical significant variables (collagen, NADH, FAD, and NADH/FAD integral area, as well as the diffuse reflectance spectra and the reduced scattering coefficient) were found.

ACKNOWLEDGMENTS

The authors would like to thank Juravinski Hospital and Cancer Centre Foundation 2014 Research Development Grant.

REFERENCES

1. Canadian Cancer Society's Advisory Committee on Cancer Statistics. Canadian Cancer Statistics 2017. Volume 2017. Toronto, ON; 2017.
2. Munshi A, Kakkar S, Bhutani R, Jalali R, Budrukkar A, Dinshaw KA. Factors influencing cosmetic outcome in Breast conservation. *Clin Oncol* 2009;21(4):285–293.
3. Breslin TM, Xu FS, Palmer GM, Zhu CF, Gilchrist KW, Ramanujam N. Autofluorescence and diffuse reflectance properties of malignant and benign breast tissues. *Ann Surg Oncol* 2004;11(1):65–70.
4. Gupta PK, Majumder SK, Uppal A. Breast cancer diagnosis using N-2 laser excited autofluorescence spectroscopy. *Lasers Surg Med* 1997;21(5):417–422.
5. Palmer GM, Zhu CF, Breslin TM, Xu FS, Gilchrist KW, Ramanujam N. Comparison of multiexcitation fluorescence and diffuse reflectance spectroscopy for the diagnosis of breast cancer (March 2003). *IEEE Trans Biomed Eng* 2003;50(11):1233–1242.
6. Zhu CF, Palmer GM, Breslin TM, Harter J, Ramanujam N. Diagnosis of breast cancer using fluorescence and diffuse reflectance spectroscopy: A Monte-Carlo-model-based approach. *J Biomed Opt* 2008;13(3):034015.
7. Volynskaya Z, Haka AS, Bechtel KL, et al. Diagnosing breast cancer using diffuse reflectance spectroscopy and intrinsic fluorescence spectroscopy. *J Biomed Opt* 2008;13(2):024012.
8. Nguyen FT, Zysk AM, Chaney EJ, et al. Intraoperative evaluation of Breast tumor margins with optical coherence tomography. *Cancer Res* 2009;69(22):8790–8796.
9. Boppart SA, Luo W, Marks DL, Singletary KW. Optical coherence tomography: Feasibility for basic research and image-guided surgery of breast cancer. *Breast Cancer Res Treat* 2004;84(2):85–97.
10. Pu Y, Tang G, Das BB, Liu CH, Pradhan A, Alfano RR. Ultrafast time-dependent fluorescence spectroscopy for human breast cancer detection. *Proceedings of SPIE*; 2012 2012 Jan 24-25; San Francisco, CA. (Proceedings of SPIE).
11. Erickson-Bhatt SJ, Nolan R, Shemonski ND, et al. In vivo intra-operative breast tumor margin detection using a portable OCT system with a handheld surgical imaging probe. *Proceedings of SPIE*; 2014 2014 Feb 02-04; San Francisco, CA. (Proceedings of SPIE).
12. Xu HN, Tchou J, Feng M, Zhao HQ, Li LZ. Differentiating cancerous from normal breast tissue by redox imaging. *Proceedings of SPIE*; 2015 Feb 07-08; San Francisco, CA. Spie-Int Soc Optical Engineering. (Proceedings of SPIE).

13. Yong WH, Butte PV, Pikul BK, et al. Distinction of brain tissue, low grade and high grade glioma with time-resolved fluorescence spectroscopy. *Front Biosci* 2006;11:1255–1263.
14. Butte PV, Fang QY, Jo JA, et al. Intraoperative delineation of primary brain tumors using time-resolved fluorescence spectroscopy. *J Biomed Opt* 2010;15(2):027008.
15. Nie ZJ, Du Le VN, Cappon D, et al. Integrated time-resolved fluorescence and diffuse reflectance spectroscopy instrument for intraoperative detection of brain tumor margin. *IEEE J Sel Topics Quantum Electron* 2016;22(3).
16. Berezin MY, Achilefu S. Fluorescence lifetime measurements and biological imaging. *Chem Rev* 2010;110(5):2641–2684.
17. Jayanthi JL, Subhash N, Manju S, Nisha UG, Beena VT. Diffuse reflectance imaging: A tool for guided biopsy. *Proceedings of SPIE*; 2012 Jan 24-25; San Francisco, CA. *Spie-Int Soc Optical Engineering*. (Proceedings of SPIE).
18. Szarko M, Muldrew K, Bertram JEA. Freeze-thaw treatment effects on the dynamic mechanical properties of articular cartilage. *Bmc Musculoskeletal Disorders* 2010; 11.
19. Nie ZJ, An R, Hayward JE, Farrell TJ, Fang QY. Hyper-spectral fluorescence lifetime imaging for optical biopsy. *J Biomed Opt* 2013;18(9):096001.
20. Chorvat D, Chorvatova A. Multi-wavelength fluorescence lifetime spectroscopy: A new approach to the study of endogenous fluorescence in living cells and tissues. *Laser Phys Lett* 2009;6(3):175–193.
21. Zhu C, Palmer GM, Breslin TM, Harter J, Ramanujam N. Diagnosis of breast cancer using diffuse reflectance spectroscopy: Comparison of a Monte Carlo versus partial least squares analysis based feature extraction technique. *Lasers Surg Med* 2006;38(7):714–724.
22. Glennie DL, Hayward JE, McKee DE, Farrell TJ. Inexpensive diffuse reflectance spectroscopy system for measuring changes in tissue optical properties. *J Biomed Opt* 2014;19(10):105005.
23. Yuan Y, Hwang JY, Krishnamoorthy M, et al. High-throughput acousto-optic-tunable-filter-based time-resolved fluorescence spectrometer for optical biopsy. *Opt Lett* 2009;34(7):1132–1134.
24. Palmer GM, Marshek CL, Vrotsos KM, Ramanujam N. Optimal methods for fluorescence and diffuse reflectance measurements of tissue biopsy samples. *Lasers Surg Med* 2002;30(3):191–200.
25. Chan E, Menovsky T, Welch AJ. Effects of cryogenic grinding on soft-tissue optical properties. *Appl Opt* 1996;35(22):4526–4532.
26. Cilesiz IF, Welch AJ. Optical-properties of human aorta—Are they affected by cryopreservation. *Lasers Surg Med* 1994; 14(4):396–402.
27. Kauppila S, Stenback F, Risteli J, Jukkola A, Risteli L. Aberrant type I and type III collagen gene expression in human breast cancer in vivo. *J Pathol* 1998;186(3):262–268.
28. Deak SB, Glaug MR, Pierce RA, et al. Desmoplasia in benign and malignant breast disease is characterized by alterations in level of messenger-rnas coding for type-I and type-III procollagen. *Matrix* 1991;11(4):252–258.
29. Skala MC, Riching KM, Bird DK, et al. In vivo multiphoton fluorescence lifetime imaging of protein-bound and free nicotinamide adenine dinucleotide in normal and precancerous epithelia. *J Biomed Opt* 2007;12(2):024014.
30. Pires L, Nogueira MS, Pratavieira S, Moriyama LT, Kurachi C. Time-resolved fluorescence lifetime for cutaneous melanoma detection. *Biomed Opt Express* 2014;5(9): 3080–3089.
31. Fang M, Yuan JP, Peng CW, Li Y. Collagen as a double-edged sword in tumor progression. *Tumor Biol* 2014;35(4): 2871–2882.
32. Provenzano PP, Inman DR, Eliceiri KW, et al. Collagen density promotes mammary tumor initiation and progression. *BMC Med* 2008;6:11.
33. Haka AS, Shafer-Peltier KE, Fitzmaurice M, Crowe J, Dasari RR, Feld MS. Diagnosing breast cancer by using Raman spectroscopy. *Proc Natl Acad Sci USA* 2005;102(35): 12371–12376.
34. Luparello C, Rizzo CP, Schillaci R. Pucciminafra i. fractionation of type-V collagen from carcinomatous and dysplastic breast in the presence of alkaline potassium-chloride. *Anal Biochem* 1988;169(1):26–32.
35. Wojcieszynska D, Hupert-Kocurek K, Guzik U. Flavin-dependent enzymes in cancer prevention. *Int J Mol Sci* 2012;13(12):16751–16768.
36. Bigio IJ, Bown SG, Briggs G, et al. Diagnosis of breast cancer using elastic-scattering spectroscopy: Preliminary clinical results. *J Biomed Opt* 2000;5(2):221–228.
37. Zhu CF, Palmer GM, Breslin TM, Harter J, Ramanujam N. Diagnosis of breast cancer using diffuse reflectance spectroscopy: Comparison of a Monte Carlo versus partial least squares analysis based feature extraction technique. *Lasers Surg Med* 2006;38(7):714–724.
38. Evers DJ, Nachabe R, Peeters MJV, et al. Diffuse reflectance spectroscopy: Towards clinical application in breast cancer. *Breast Cancer Res Treat* 2013;137(1):155–165.
39. Yu B, Shah A, Nagarajan VK, Ferris DG. Diffuse reflectance spectroscopy of epithelial tissue with a smart fiber-optic probe. *Biomed Opt Express* 2014;5(3):675–689.
40. Ghosh N, Mohanty SK, Majumder SK, Gupta PK. Measurement of optical transport properties of normal and malignant human breast tissue. *Appl Opt* 2001;40(1): 176–184.
41. Vishwanath K, Chang K, Klein D, et al. Portable, fiber-based, diffuse reflection spectroscopy (DRS) systems for estimating tissue optical properties. *Appl Spectrosc* 2011; 65(2):206–215.